Cancer Chemother Pharmacol
DOI 10.1007/s00280-015-2795-7

ORIGINAL ARTICLE

Validation of a predictive modeling approach to demonstrate the relative efficacy of three different schedules of the AKT inhibitor AZD5363

James W. T. Yates[1] · Phillippa Dudley[1] · Jane Cheng[2] · Celina D'Cruz[2] · Barry R. Davies[1]

Received: 6 March 2015 / Accepted: 28 May 2015

Abstract
Purpose Intermittent dosing of inhibitors of the PI3K/AKT/mTOR network offers the potential to maximize the therapeutic margin. Here, we validate a predictive modeling approach to establish the relative efficacy of continuous and two intermittent dosing schedules of the AKT inhibitor AZD5363.
Methods A mathematical model of pharmacokinetics, pharmacodynamics and anti-tumor effect was constructed based upon experimental data from dosing regimens that give constant and transient inhibition of the AKT pathway.
Results Continuous and intermittent dosing of AZD5363 inhibited growth of BT474c xenografts and caused dose- and time-dependent inhibition of AKT substrate phosphorylation. Both dosing schedules inhibited proliferation, but a higher intermittent dose also induced apoptosis. The mathematical model described this pharmacodynamic and efficacy data well, for both monotherapy and combination dosing with docetaxel, and predicted that equivalent efficacy could be achieved at 1.3- and 1.7× continuous dose when AZD5363 was dosed intermittently for 4 and 2 days per week, respectively. These predictions were confirmed in two independent xenograft models. Moreover, the model also correctly predicted the relative efficacy of three different sequences of intermittent dosing of AZD5363 with docetaxel.
Conclusions Equivalent anti-tumor activity to continuous dosing can be achieved at modestly increased intermittent doses of AZD5363. These intermittent dosing regimens may potentially overcome tolerability issues seen with continuous dosing and enable greater flexibility of dosing schedule in combination with other agents, including chemotherapy.

Keywords PKPD · Combination therapy · Kinase inhibitors · Mathematical modeling

Introduction

The signaling network containing PI3K, AKT and mTOR is the most frequently mutated in human cancer. AKT is a central node in this signaling network, with a range of substrates controlling growth, apoptosis and metabolism [1]. Two distinct types of relatively selective AKT inhibitor are being tested in the clinic. Allosteric inhibitors such as MK-2206 bind to the region that interacts with both the PH and kinase domains and prevent translocation of AKT to the membrane and activation. This group is exemplified by MK-2206 [2]. Classical ATP-competitive catalytic inhibitors, which prevent substrate phosphorylation by AKT, have also been developed. This latter group includes AZD5363, a potent pan AKT kinase inhibitor with pharmacodynamic properties consistent with mechanism in vivo, and anti-tumor activity in xenograft models with PIK3CA and PTEN mutations [3].

The majority of signaling inhibitors that have been registered to treat cancer patients are dosed continuously or near-continuously. This is also true of inhibitors targeting

Electronic supplementary material The online version of this article (doi:10.1007/s00280-015-2795-7) contains supplementary material, which is available to authorized users.

✉ James W. T. Yates
james.yates@astrazeneca.com

[1] Oncology iMED, AstraZeneca, Alderley Park, Mereside, Macclesfield, Cheshire SK10 4TG, UK

[2] Oncology iMED, AstraZeneca, Gatehouse Park, Waltham, MA, USA

Published online: 20 June 2015

PI3K and AKT that are currently in development. Hence, the established paradigm for cancer pathway signaling inhibitors is to inhibit the target as continuously as possible. Moreover, the long half-life of many compounds, including the AKT inhibitors MK-2206 [4] and GDC-0068 [5], may limit the scope for investigating higher, intermittent doses. While continuous target inhibition may be advantageous if the mechanism of action of the drug is primarily to slow or arrest the cell cycle, it is possible that higher intermittent doses may be more effective at inducing apoptosis, whether as monotherapy or in combination with cytotoxic drugs, the majority of which are dosed using intermittent schedules. Furthermore, intermittent dosing schedules also provide flexibility to avoid antagonism between agents [6] and may enable the avoidance of dose-limiting toxicities that arise as a consequence of continuous dosing [7, 8]. This concept has been exemplified preclinically by intermittent dosing schedules of the EGFR inhibitor gefitinib in combination with paclitaxel in NSCLC xenografts [9, 10], sorafenib in 786-0 RCC xenografts [11] and the Jak2 inhibitor MRLB-11055 in mouse models of polycythemia vera [12], and in the clinic for gefitinib and erlotinib in combination with docetaxel [13, 14], and dasatinib in imatinib-resistant chronic-phase CLL [8, 15].

We now report on the adoption and validation of a predictive modeling approach to determine intermittent dosing schedules that deliver equivalent efficacy to that resulting from continuous dosing of the AKT inhibitor AZD5363. An approach is also illustrated to elucidate the schedule dependence of anti-tumor activity in breast cancer xenografts treated with a combination of docetaxel and AZD5363. Simeoni et al. [16] published a mathematical model, widely used in preclinical experimentation to describe the growth and inhibition by anticancer agents of xenografted models, while Ribba et al. [17] demonstrated the utility of a mechanistic model that characterizes the tumor xenograft in terms of non-hypoxic, hypoxic and necrotic regions. In this paper, we will illustrate modeling approaches that have been utilized when the simplifying assumptions in the Simeoni model (linear drug effect, cytotoxic mechanism of action) are invalid, and extend the model presented by Ribba et al., to incorporate the spatial features of a tumor in an attempt to better describe the tumor microenvironment [18].

Methods

Animals

Specific, pathogen-free, female nude mice were bred at AstraZeneca (Alderley Park, UK) and housed in pathogen-free conditions. Animals were maintained in rooms under controlled conditions of temperature (19–23 °C), humidity (55 ± 10 %), photoperiod (12-h light/12-h dark) and air exchange. Animals were housed in standard cages within a flexible film isolator, with food and water provided ad libitum. The facilities have been approved by the Home Office License and meet all current regulations and standards of the UK. The mice were used between the ages of 8 and 12 weeks in accordance with institutional guidelines.

Implantation of cells into mice

For in vivo implants, cells were harvested from T225 tissue culture flasks by a 2- to 5-min treatment with 0.05 % trypsin (Invitrogen) in EDTA solution followed by suspension in basic medium and three washes in phosphate-buffered saline (Invitrogen). Only single-cell suspensions of greater than 90 % viability, as determined by trypan blue exclusion, were used for injection. Tumor cells were injected subcutaneously in the left flank of the animal in a volume of 0.1 mL. For BT474c studies, the animals were supplemented with 0.36 mg/60 day 17β-estradiol pellets (Innovative Research of America) 1 day prior to cell implantation.

Efficacy studies

When mean tumor size reached approximately 0.2 cm^3, the mice were randomized into control and treatment groups. The treatment groups received varying dose schedules of AZD5363 solubilized in a 10 % DMSO 25 % w/v Kleptose HPB (Roquette) buffer by oral gavage, docetaxel (Sanofi-Aventis) solubilized in 2.6 % ethanol in injectable water by intravenous injection once on day 1 at 15 or 5 mg/kg once weekly. When administered in combination, the cytotoxic was administered 1 h prior to the oral dose of AZD5363. The control group received the DMSO/Kleptose buffer alone, twice daily by oral gavage. Tumor volumes (measured by caliper), animal body weight and tumor condition were recorded twice weekly for the duration of the study. Mice were humanely killed by CO_2 euthanasia. The tumor volume was calculated (taking length to be the longest diameter across the tumor and width to be the corresponding perpendicular diameter using the formula: (length × width) × $\sqrt{}$(length × width) × (π/6)). This volume formula assumes that the tumors are spherical in shape and enables calculation of volume from vernier caliper measurements of two dimensions.

Pharmacodynamic studies

When mean tumor size reached 0.2–0.5 cm^3, the mice were randomized into control ($n = 8$ animals) and treatment groups ($n = 5$ animals per group). The treatment

groups received 300 or 100 mg/kg acute dose of AZD5363 solubilized in a DMSO/Kleptose buffer, by oral gavage. The control group received the DMSO/Kleptose buffer alone, once by oral gavage. At various time points after dosing, the animals were humanely killed and the samples collected. Half the tumor was snap-frozen in liquid nitrogen and stored at −80 °C for pharmacodynamic analysis; the other half was fixed in 10 % formalin buffer for 24 h and then embedded in paraffin for immunohistochemical (IHC) staining. Total blood was collected by intracardiac puncture, and plasma was prepared and immediately frozen at −20 °C for pharmacokinetic analysis. Frozen tumors were homogenized using Fastprep methodology lysis matrix A (MP Biomedicals), and lysates were generated using adjusted lysis buffer (1 % TritonX-100). Equivalent amounts of protein (12 µg/lane) were resolved by 4–15 % gradient SDS-polyacrylamide premade gels (#345-0035 Bio-Rad) and transferred to nitrocellulose membranes. Membranes were then incubated with primary antibodies, total GSK3β (BD Transduction Labs. #610202), phosphorylated GSK3β (Cell Signaling Technology #9336), total S6 (Cell Signaling Technology #2217), phosphorylated S6 (Cell Signaling Technology #2211), and subsequently with horseradish peroxidase-conjugated anti-mouse IgG (Cell Signaling Technology #7076) or anti-rabbit IgG (#7074) diluted in 5 % powdered milk (Marvel™) in PBS. Immunoreactive proteins were detected by enhanced chemiluminescence (#34080 Pierce) and bands quantified with a ChemiGenius (Syngene). Phosphorylated PRAS40 was measured using solid-phase sandwich ELISA (Biosource #KHO0421). Ki67 and cleaved caspase 3 were measured by IHC. Antigen retrieval was carried out by placing sections in low pH antigen retrieval solution (Dako #S1699) in a pressure vessel and heating to 110 °C in a microwave oven. Following blocking of endogenous peroxidase, slides were stained with a mouse monoclonal antibody to Ki67 (Dako M7240) or rabbit polyclonal antibody to cleaved caspase 3 (CST #9661) and visualized with the appropriate HRP-linked secondary antibody and DAB. Sections were counterstained with hematoxylin. Image analysis was carried out using ScanScope. Briefly, regions of interest were annotated to exclude areas of background staining or poor sample quality. Appropriate image analysis algorithms were tuned for each marker (nuclear algorithm for Ki67; color deconvolution algorithm for cleaved caspase 3), and the entire viable region was analyzed for each sample. For Ki67, the total percent positive nuclei were scored, and for cleaved caspase 3, the percent total positivity was recorded. Statistical differences between treatment groups were analyzed by one-way ANOVA, and p values of <0.05 corresponding to t test based on pooled variances were considered significant.

Mathematical model

The Simeoni [16] and Ribba [17] models were adapted to incorporate features that describe: (1) the utility of biomarkers proximal to the target in cell signaling pathways as a driver for growth inhibition; (2) multiple mechanisms of drug action on subpopulations of cells that drive tumor growth. The resulting tumor growth model [18] shown in Fig. 1b incorporates the concepts of a "shell" of cells, sufficiently proximal to blood vessels to be cycling; a hypoxic layer with the potential to cycle; a necrotic core. It was assumed that pS6 levels were predictive of the rate of proliferation, so that a reduction in pS6 levels would result in a slower tumor growth rate. S6 is downstream of mTOR;

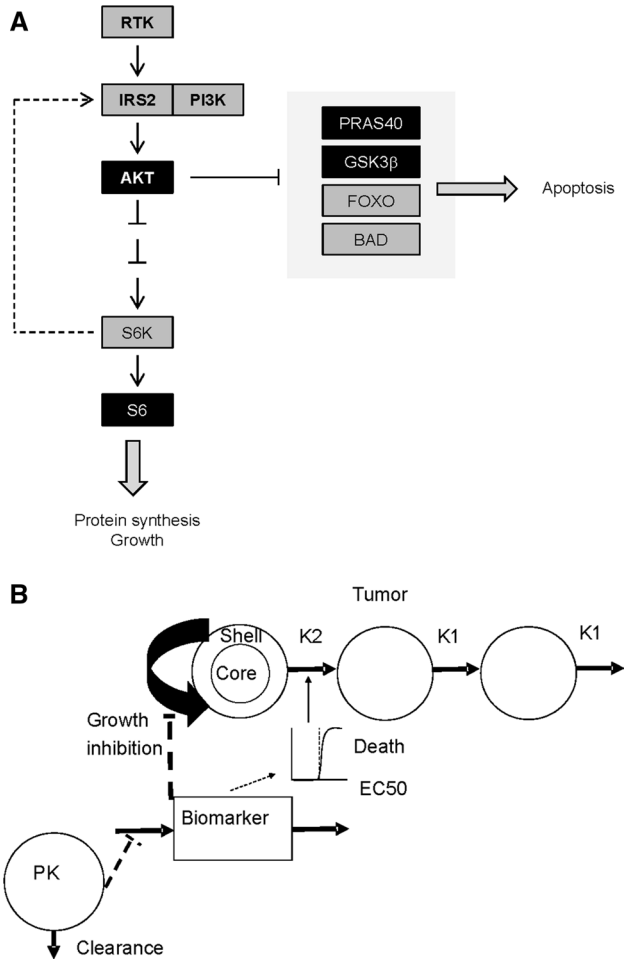

Fig. 1 Schematic diagrams of the pathway and model that integrates pharmacokinetics, pathway biomarkers and efficacy for AZD5363. **a** Simplified model of the PI3K-AKT pathway. Measured biomarkers are indicated in *black boxes,* and the negative feedback loop from S6K is indicated with a *dashed line*. **b** Schematic of model that integrates pharmacokinetics, pathway biomarkers and efficacy. Biomarker inhibition leads to growth inhibition and ultimately, when a threshold pathway inhibition is achieved, cell death. Docetaxel effect on K2 is also incorporated

it controls initiation of protein synthesis and is a key regulator of cell growth [19]; moreover, levels of pS6 have been correlated with biomarkers of cell proliferation such as Ki67 and MIB1 in clinical samples from a number of tumor types, e.g., glioma [20]. The phosphorylation status of GSK3β was used as a surrogate of pro-survival signaling because it is one of several direct substrates of AKT that are known to regulate apoptosis. It was therefore assumed that an increase in unphosphorylated GSK3β (inferred from a reduction in phosphorylated GSK3β) would result in an increased rate of apoptosis. While the role of GSK3β itself in apoptosis is controversial, other direct AKT substrates including forkhead transcription factors (FOXOs), XIAP and BAD are well-established regulators of apoptosis [1], and PRAS40 is known to deregulate apoptosis in malignant melanoma [21]. The details of the mathematical model can be found in the supplementary material. Its components are described briefly below.

PK model for AZD5363

A two-compartment model with first-order absorption was used to model the pharmacokinetics of AZD5363 in the mouse. Dose-dependent changes (data not shown) were noted in the absorption kinetics and were so modeled as having an absorption rate dependent upon the gut concentration of the compound.

$$K_a = K_{\text{peff}} - \left(\frac{V\max}{K_m + \text{GUT}}\right)$$
$$\frac{\text{dGUT}}{\text{d}t} = -K_a\text{GUT}$$
$$\frac{\text{dCEN}}{\text{d}t} = -\left(\frac{(Q + \text{CL})}{V_1}\right)\text{CEN} + \left(\frac{Q}{V_2}\right)\text{PER} + K_a\text{GUT}$$
$$\frac{\text{dPER}}{\text{d}t} = Q\left(\frac{\text{CEN}}{V_1} - \frac{\text{PER}}{V_2}\right)$$
$$C_{\text{p}} = \frac{\text{CEN}}{V_1}$$

where GUT is the oral dose compartment, CEN is the observed blood compartment, PER is a peripheral compartment, C_{p} is the predicted plasma concentration of AZD5363.

Parameter estimates as well as explanations of parameters are presented in Table S1 for fits to data resulting from dosing 2 mg/kg iv as well as a range of oral dosing. Standard errors were derived by inverting the Fisher information matrix associated with the regression problem and are very small, reflecting that parameters are well determined.

PK model for docetaxel

Docetaxel pharmacokinetics were described by a linear two-compartment model.

$$\frac{\text{dCEN}_{\text{tax}}}{\text{d}t} = -\left(\frac{(Q_{\text{tax}} + \text{CL}_{\text{tax}})}{V_{1,\text{tax}}}\right)\text{CEN}_{\text{tax}} + \left(\frac{Q_{\text{tax}}}{V_{2,\text{tax}}}\right)\text{PER}_{\text{tax}}$$
$$\frac{\text{dPER}_{\text{tax}}}{\text{d}t} = Q_{\text{tax}}\left(\frac{\text{CEN}_{\text{tax}}}{V_{1,\text{tax}}} - \frac{\text{PER}_{\text{tax}}}{V_{2,\text{tax}}}\right)$$
$$C_{\text{tax}} = \frac{\text{CEN}_{\text{tax}}}{V_{1,\text{tax}}}$$

where C_{tax} is the predicted plasma concentration of docetaxel. Parameter estimates are detailed in Table S2. Standard errors were derived by inverting the Fisher information matrix associated with the regression problem and are of an acceptable size.

Pathway model

A simple pathway model (Fig. 1a) was developed to link the dynamics of the various pathway biomarkers. This model is based upon mass action and describes the phosphorylation and dephosphorylation of the kinases modeled. This model incorporates the negative feedback mediated by S6K and IRS1 onto PI3K, with the modeled pS6 being used as a surrogate for this. The S6K-negative feedback loop to IRS1/2 is well described in the literature [23].

Define:

$$k_{\text{AKT}} = \frac{1 - \text{AKT}_{\text{ph,control}}}{\text{AKT}_{\text{ph,control}}}$$
$$k_{\text{S6}} = \frac{1 - \text{S6}_{\text{ph,control}}}{\text{S6}_{\text{ph,control}}}$$
$$k_{\text{GSK3}\beta} = \frac{1 - \text{GSK3}\beta_{\text{ph,control}}}{\text{GSK3}\beta_{\text{ph,control}}}$$
$$k_{\text{PRAS40}} = \frac{1 - \text{PRAS40}_{\text{ph,control}}}{\text{PRAS40}_{\text{ph,control}}}$$
$$k_{e0} = \frac{\ln(2)}{\text{EffHalf}}$$

here, for example, $\text{AKT}_{\text{ph,control}}$ is the fraction of AKT molecules phosphorylated at baseline. Thus, the parameters, k_{AKT}, etc., define the baseline ratio of phosphorylated to unphosphorylated protein. Define the fraction of AKT molecules without AZD5363 bound as $f_u = \frac{k_{\text{drug}}}{k_{\text{drug}} + C_e}$.

Then, the differential equations for the biomarkers are as follows

$$\frac{\mathrm{dAKT_{ph}}}{\mathrm{d}t} = k_{\mathrm{ph,AKT}}\left(\left(1-\mathrm{AKT_{ph}}\right)\left(\frac{S6_{\mathrm{ph,control}}}{S6_{\mathrm{ph}}}\right) - k_{\mathrm{AKT}} f_u \mathrm{AKT_{ph}}\right)$$

$$\frac{\mathrm{dS6_{ph}}}{\mathrm{d}t} = k_{\mathrm{ph,S6}}\left(\left(1-\mathrm{S6_{ph}}\right)\left(\frac{\mathrm{AKT_{ph}}}{\mathrm{AKT_{ph,control}}}\right) f_u - k_{\mathrm{S6}}\mathrm{S6_{ph}}\right)$$

$$\frac{\mathrm{dGSK3\beta_{ph}}}{\mathrm{d}t} = k_{\mathrm{ph,GSK3b}}\left(\left(1-\mathrm{GSK3\beta_{ph}}\right)\left(\frac{\mathrm{AKT_{ph}}}{\mathrm{AKT_{ph,control}}}\right) f_u - k_{\mathrm{S6}}\mathrm{GSK3\beta_{ph}}\right)$$

$$\frac{\mathrm{dPRAS40_{ph}}}{\mathrm{d}t} = k_{\mathrm{ph,PRAS40}}\left(\left(1-\mathrm{GSK3\beta_{ph}}\right)\left(\frac{\mathrm{AKT_{ph}}}{\mathrm{AKT_{ph,control}}}\right) f_u - k_{\mathrm{S6}}\mathrm{GSK3\beta_{ph}}\right)$$

Here the k_{ph} parameters are the rate of dephosphorylation. The model can then be compared to the fraction of control data generated experimentally thus:

$$\mathrm{AKT_{ph,nf}} = 100 * \left(\frac{\mathrm{AKT_{ph}}}{\mathrm{AKT_{ph,control}}}\right)$$

$$\mathrm{S6_{ph,nf}} = 100 * \left(\frac{\mathrm{S6_{ph}}}{\mathrm{S6_{ph,control}}}\right)$$

$$\mathrm{GSK3\beta_{ph,nf}} = 100 * \left(\frac{\mathrm{GSK3\beta_{ph}}}{\mathrm{GSK3\beta_{ph,control}}}\right)$$

$$\mathrm{PRAS40_{ph,nf}} = 100 * \left(\frac{\mathrm{PRAS40}_{ph}}{\mathrm{PRAS40_{ph,control}}}\right)$$

The subscript nf stands for normalized fraction and reflects that the data as presented are normalized to control phosphorylation fraction.

Linkage between PD and efficacy

It is assumed that

1. pS6 is a marker of potential to proliferate,
2. unphosphorylated GSK3β is a marker of the potential for apoptosis.

The change of biomarker from control is defined thus:

$$\mathrm{GSK3\beta}_u = 1 - \mathrm{GSK3\beta_{ph}}$$

$$\mathrm{GSK3\beta}_{u,\mathrm{control}} = 1 - \mathrm{GSK3\beta_{ph,control}}$$

$$\mathrm{GSK3\beta_{change}} = \max\left(0, \frac{\left(\mathrm{GSK3\beta}_u - \mathrm{GSK3\beta}_{u,\mathrm{control}}\right)}{\mathrm{GSK3\beta}_{u,\mathrm{control}}}\right)$$

$$\mathrm{S6_{change}} = \frac{\mathrm{S6_{ph}}}{\mathrm{S6_{ph,control}}}$$

The change of biomarker is linked to changes in tumor growth, thus:

$$\mathrm{GrowthRate} = \mathrm{S6_{change}} k_{\mathrm{grow}}$$

$$\mathrm{KillRate} = \left(\frac{k_{\mathrm{kill}}\mathrm{GSK3\beta}^N_{\mathrm{change}}}{k^{\mathrm{N}}_{\mathrm{threshold}} + \mathrm{GSK3\beta}^N_{\mathrm{change}}}\right)$$

The linkage between unphosphorylated GSK3β and apoptosis is modeled as a threshold relationship (the parameter N defines how steep the relationship is).

Docetaxel effect

In the absence of biomarker data from dosing docetaxel in BT474 xenografts, a linkage was made between PK and efficacy. The effects of AZD5363 on the substrates of AKT are incorporated in order to allow for a synergistic effect via reduced survival signaling. It was further assumed that docetaxel only affects cycling cells within the tumor, and thus, the effect should be proportional to the growth rate of the tumor. AZD5363 is assumed to reduce this rate, and so the model incorporates the potential for the antagonism of drug effect.

$$\mathrm{KillRate_{tax}} = \mathrm{GrowthRate} \cdot k_{\mathrm{tax}} \cdot C_{\mathrm{tax}}\left(\mathrm{GSK3\beta_{change}}\right)^{\mathrm{Ninter}}$$

Here Ninter is a power term measuring the influence AD5363-induced GSK3β changes have on the efficacy of docetaxel.

Tumor growth model

The model used is an adaptation of a model previously reported [18] where the tumor is modeled as a sphere. The model assumes that the tumor is structured so that the proliferating compartment is confined to the outer parts of the tumor: Reflecting capacity limited delivery of blood from the host to the tumor, reflecting more directly the pathophysiology of a tumor. It is assumed that this "shell" maintains a constant depth (R_{diff}) as the tumor grows. This results in a set of equations larger than other models reported [22]; however, it should be noted that there are still only three parameters for control growth. The advantage of this model is that it provides a modeled proliferating fraction which we assume is the fraction impacted by docetaxel. This allows us to model the combination in a mechanistic manner. The model is initialized as follows:

The initial tumor radius is calculated:

$$\text{rtot}_0 = \left(\frac{3\text{Vol}_0}{4\Pi}\right)^{1/3}$$

The initial volume is then assigned to the proliferating shell and the quiescent core dependent on whether rtot_0 is greater than R_{diff}.

If $\text{rtot}_0 > R_{\text{diff}}$, then

$$\text{rcore}_0 = \text{rtot}_0 - R_{\text{diff}}$$
$$\text{shell}V_0 = \left(\frac{4\Pi}{3}\right)\left(\text{rtot}_0^3 - \text{rcore}_0^3\right)$$
$$\text{core}V_0 = \left(\frac{4\Pi}{3}\right)\left(\text{rcore}_0^3\right)$$

otherwise the total initial volume is in the proliferating shell:

$$\text{shell}V_0 = \left(\frac{4\Pi}{3}\right)\left(\text{rtot}_0^3\right)$$
$$\text{core}V_0 = 0$$

The volumes of the shell and core of the tumor over time are defined as follows:

$$\text{shell}V = S_a + S_{d1} + S_{d2} + S_{d3}$$
$$\text{core}V = C_a + C_{d1} + C_{d2} + C_{d3}$$
$$V = \text{shell}V + \text{core}V$$

Here the subscript "*a*" is for "alive cells" with the potential to proliferate, and subscripts $d1$ to $d3$ are cells that are undergoing apoptosis. Consequently, the radii of the compartments are defined over time as follows:

$$\text{rtot} = \left(\frac{3V}{4\Pi}\right)^{1/3}$$
$$\text{rcore} = \left(\frac{3\text{core}V}{4\Pi}\right)^{1/3}$$

In order for the proliferation shell compartment to maintain a constant depth, as the tumor changes volume, some of the tumor volume will have to be reassigned between the shell and core. The total volume movement if the current tumor radius is greater than R_{diff} is

$$\text{Transfer\_Rate} = \frac{\text{d}V}{\text{d}t}\left(\frac{\text{rtot} - R_{\text{diff}}}{\text{rtot}}\right)^2 + K_{\text{ex}}C_{d3},$$

where

$$\frac{\text{d}V}{\text{d}t} = (\text{GrowthRate} - \text{DeathRate})S_a - K_{\text{ex}}(S_{d3} + C_{d3})$$

otherwise Transfer_Rate = 0.

The differential equations for the tumor over time are defined as follows:

$$\frac{\text{d}S_a}{\text{d}t} = (\text{GrowthRate} - \text{KillRate} - \text{KillRate}_{\text{Tax}})S_a - f_a\text{Transfer\_Rate}$$
$$\frac{\text{d}S_{d1}}{\text{d}t} = \text{KillRate}_{\text{Tax}}S_a - K_{\text{ex}}S_{d1} - f_{d1}\text{Transfer\_Rate}$$
$$\frac{\text{d}S_{d2}}{\text{d}t} = K_{\text{ex}}(S_{d1} - S_{d2}) - f_{d2}\text{Transfer\_Rate}$$
$$\frac{\text{d}S_{d3}}{\text{d}t} = K_{\text{ex}}(S_{d2} - S_{d3}) - f_{d3}\text{Transfer\_Rate}$$

The core is defined similarly:

$$\frac{\text{d}C_a}{\text{d}t} = f_a\text{Transfer\_Rate}$$
$$\frac{\text{d}C_{d1}}{\text{d}t} = -K_{\text{ex}}C_{d1} + f_{d1}\text{Transfer\_Rate}$$
$$\frac{\text{d}C_{d2}}{\text{d}t} = K_{\text{ex}}(C_{d1} - C_{d2}) + f_{d2}\text{Transfer\_Rate}$$
$$\frac{\text{d}C_{d3}}{\text{d}t} = K_{\text{ex}}(C_{d2} - C_{d3}) + f_{d3}\text{Transfer\_Rate}$$

Here f_x is the fraction that a given compartment (a, $d1$, $d2$ or $d3$) is of the donating physiological compartment (shell or core): If the tumor is growing, the shell is donating to the core.

Parameter estimation and software

All modelings and simulations were carried out in ACSLX version 3.0 (The Aegis Technologies Group, Huntsville, Alabama, USA). Parameters were estimated using a maximum likelihood framework, with an appropriate measurement noise distribution for each data type being assumed. Significance of allowing the interaction parameter Ninter to vary from 0 was determined by the resulting drop in the log-likelihood function (LLF) when it was included. It was assumed that the change in the LLF was distributed as a χ^2 distribution with one degree of freedom. This assumption was justified because nested models were compared with the addition of one interaction parameter.

Results

High intermittent dosing of AZD5363 induces apoptosis

The pharmacokinetics of AZD5363 in mouse were used to set two dosing regimens that delivered approximately the same drug exposure per week but with continuous exposure vs high intermittent exposure. The regimens chosen were 100 mg/kg twice daily continuous (1400 mg/

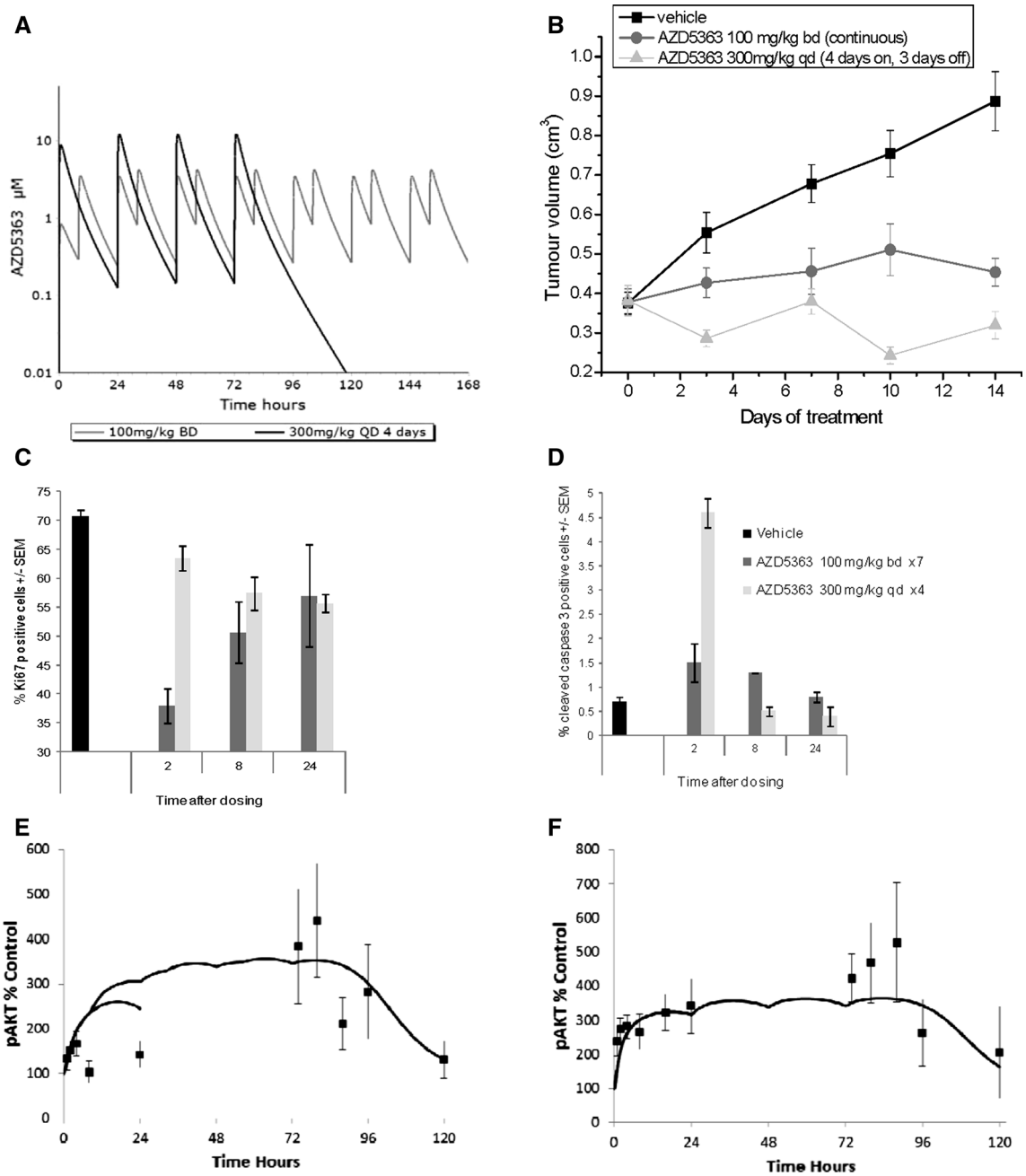

Fig. 2 Actual and modeled data showing pharmacokinetics, pharmacodynamics and anti-tumor activity of AZD5363 in BT474c xenografts. **a** Simulation of pharmacokinetics based upon prior data used to choose continuous and intermittent schedules that gave the same AUC per week but different Cmax and duration of exposure. **b** Anti-tumor activity in BT474c xenografts following chronic dosing of 100 mg/kg bid continuous dosing and 300 mg/kg qd 4 days on, 3 days off. **c**, **d** Immunostaining for Ki67 and cleaved caspase 3, respectively, at indicated time points following 4 days of short-term chronic dosing at 100 mg/kg bid and 300 mg/kg QD. **e**–**l** Corresponding pathway pharmacodynamics at 100 mg/kg BD (**e**, **g**, **i**, **k**) and 300 mg/kg QD (**f**, **h**, **j**, **l**) and model fit. Data are shown as means at each time point with standard error of the mean, and model fits for single and repeat dosing are *solid lines*

kg/week) and 300 mg/kg once daily for 4 days in a week (1200 mg/kg/week). The simulations of the mean pharmacokinetic profiles are shown in Fig. 2a. When tested in the BT474c xenografted tumors, different patterns of tumor growth were observed (Fig. 2b) with the intermittent schedule resulting in waves of regression during the dosing period and regrowth in the dosing holiday period. The continuous regimen resulted in a slowed growth of tumors

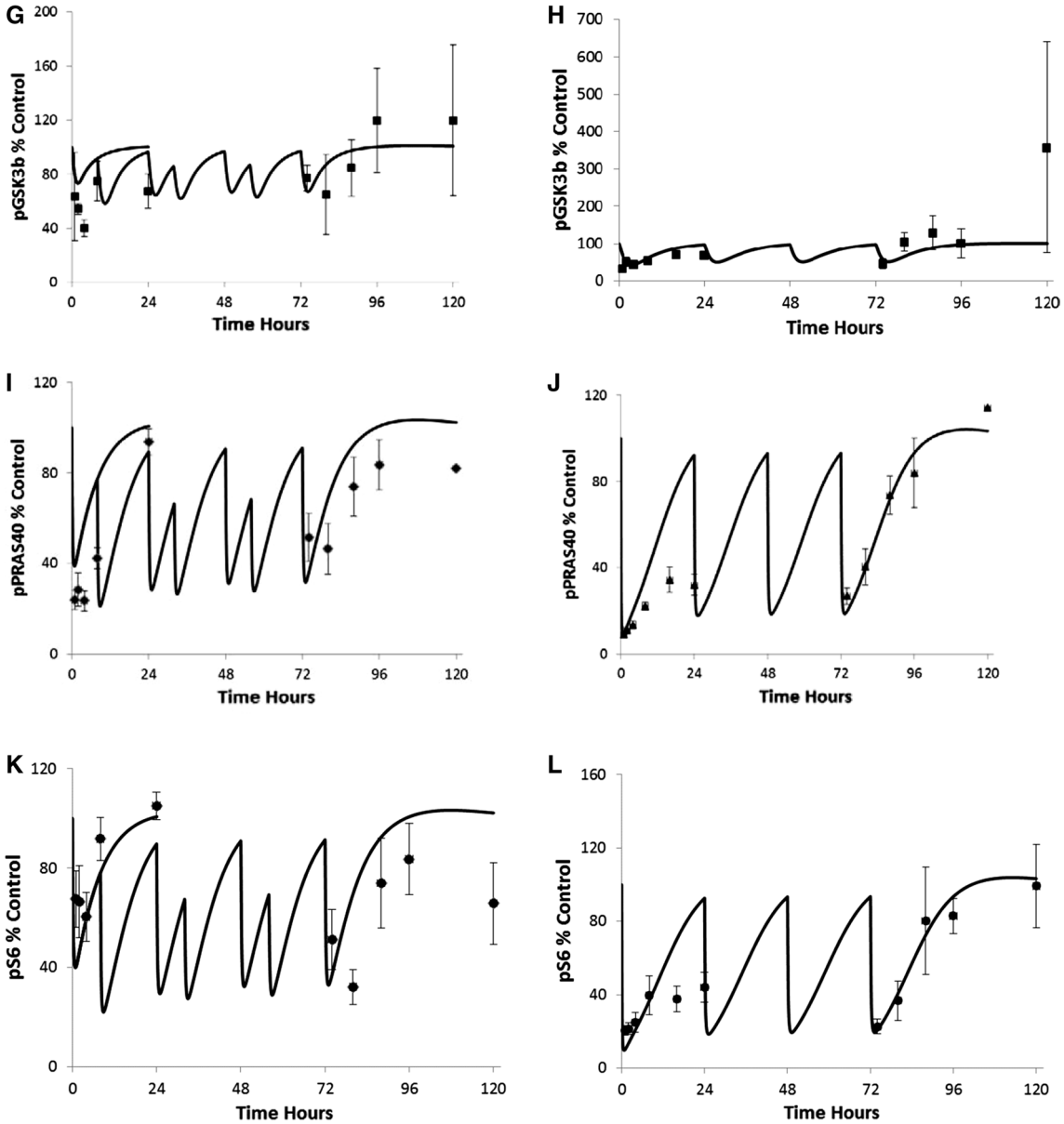

Fig. 2 continued

compared to control. Both dosing schedules were well tolerated; mean body weight loss did not exceed 6 % and was not significantly different in the two groups, and no overt toxicity was observed. Interestingly, a different mechanism of action appeared to be invoked by the high intermittent dose. Both regimens caused a reduction in Ki67 staining, which achieved statistical significance at 24 h after the final dose of 300 mg/kg qd and at all time points after the final dose of 100 mg/kg bid (Fig. 2c), indicating a reduction in proliferating cells. However, only the intermittent schedule induced a significant increase in cleaved caspase 3 staining, detectable at 2 h after the final dose, indicative of apoptosis (Fig. 2d).

Pathway biomarker changes after dosing with AZD5363 can be explained with a mathematical model

In order to quantitatively investigate the differences between these regimens in the BT474c xenograft model, the phosphorylation of AKT, its substrates PRAS40 and GSK3β, and the downstream pathway biomarker S6 were measured at a number of time points after single doses of 100 and 300 mg/kg and 4 days after short-term chronic doses of 100 mg/kg twice daily and 300 mg/kg once daily. Figure 2e, f shows the increase in pAKT after 100 and 300 mg/kg doses, respectively, while Fig. 2g–l shows

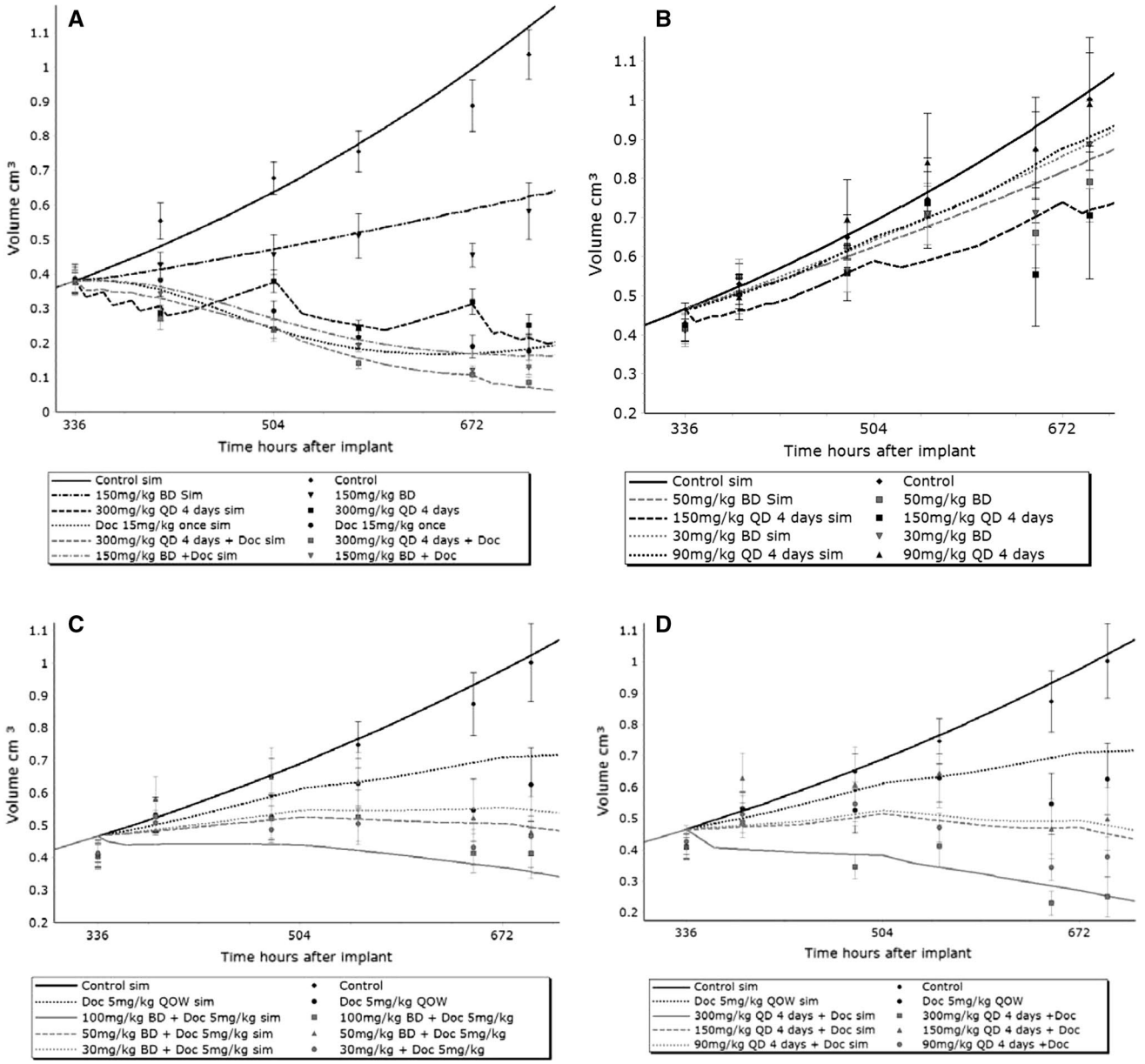

Fig. 3 Calibration of efficacy model parameters using BT474c tumor growth data. The modeled data (*bold solid* and *dashed lines*) were able to reproduce measured monotherapy and combination anti-tumor effects (*points plus error bars*) for a variety of doses and regimens

the reduction in phosphorylation of the substrates of AKT and S6. Here, observed data are shown as points with error bars, representing mean ± standard error of mean. A mathematical model of the relationships between these markers was constructed as described in "Materials and Methods" (Fig. 1a) and parameterized using the data. The resulting fit (Fig. 2e–l; solid lines) demonstrates the model to be adequate. Based upon the standard errors of the estimates, robust parameter estimates resulted (Table S3). Specifically, the model could simultaneously capture the increase in pAKT as well as the dose- and time-dependent reduction in the phosphorylation of the substrates of AKT and S6.

Relationship between biomarker changes and tumor growth changes for different regimen can be described using a mathematical model

Given that marked differences in the tumor growth over time were observed for intermittent versus continuous dosing, a model-based investigation into the relationship between pathway inhibition and tumor growth over time was carried out. To this end, the pathway model reported above was incorporated into a mathematical model of tumor growth that has been previously reported [18]. Changes in the phosphorylation of substrates of AKT were

used as surrogates of phenotypic changes (proliferation and apoptosis) as described in the "Methods" section.

The data from a dose fractionation experiment were used first to parameterize the model, and these data consisted of AZD5363 dosed either continuously twice daily or 4 days on/3 days off once daily, as monotherapy and in combination with docetaxel, in BT474c xenografts. The measured data and model fits are shown in Fig. 3a, and the parameter estimates are reported in Table S4. The model captured both the differences between the dosing regimen and the combination effect well. The residual error was 17 % again demonstrating a good correspondence between model and data.

To investigate the relationship further, dose–response studies were performed in the same BT474c xenograft model, investigating different dosing levels of the same continuous and intermittent schedules of dosing as monotherapy and in combination with docetaxel (Fig. 3b–d). Again the model described the data well with relatively modest changes in parameters (Table S4) in comparison with the original study (Table S3). Again the residual error, at 19 %, demonstrated a good correspondence between model and data.

Dose-sequencing experiments demonstrate synergism and antagonism that are captured by the mathematical model

Up to this point, a fixed sequence of docetaxel was used in all of the experiments, in which docetaxel was administered 1 h before the first dose of AZD5363 in each weekly cycle. The mathematical model assumes the potential for antagonism due to AZD5363 reducing the rate of tumor cell proliferation and by implication the M-phase fraction; this may reduce the effectiveness of docetaxel if the chemotherapy is dosed at the end of an intermittent cycle of AZD5363. It was decided to investigate the relationship between dosing sequence and efficacy when docetaxel is combined with 4 days 300 mg/kg QD AZD5363. Three sequences were considered: AZD5363 for the 4 days before docetaxel; AZD5363 dosing starting 1 h after docetaxel on the day the chemotherapy is administered; and AZ5363 dosing starting on the day after docetaxel is administered. The data and model fits are shown in Fig. 4a. The model captures the rank order of the effectiveness of the various sequences, although the subsequent tumor growth after cessation of dosing of AZD5363 followed by docetaxel is not completely captured. The parameter estimates are shown in Table S5. Interestingly, with this data set, a small, but statistically significant, synergistic interaction was inferred between AZD5363 and docetaxel as characterized by the parameter Ninter. The relative effectiveness of the three different dosing schedules of AZD5363 in combination with chemotherapy was confirmed in a different breast cancer xenograft model. In HCC-1187 xenografts, frank antagonism was seen when docetaxel was administered after the 4 days of AZD5363 intermittent dosing, while administration of docetaxel the day before or on the same day as the first dose of AZD5363 was equally effective at inducing tumor regression (Fig. 4b).

Interrogation of the mathematical model results in relationship between dose intensity, duration and efficacy in BT474c xenografts

A simulation study was set up to infer from the mathematical model the relationship between days dosing per week and the fold dose increase required to achieve the same end of study tumor growth inhibition compared to dosing every day in the week. Figure 5a shows the simulated relationship between schedule and dose to achieve the same efficacy as continuous dosing (a form of dose–schedule isobole). It was found that the model predicted that a 30 % unit dose increase was required for the 4 days a week schedule and a 70 % increase was required for 2 days per week schedule. Importantly (Fig. 5b), the model simulations showed that the same efficacy could be achieved on intermittent schedules while reducing the overall drug burden. The same relationship was found to hold for the combination regimen of docetaxel followed by AZD5363.

Experimental validation of predicted equi-efficacious regimens

Further efficacy studies were carried out to validate these modeling predictions. The relative efficacy of continuous, 4 days on/3 days off and 2 days on/5 days off schedules using doses of AZD5363 predicted to be equally efficacious was compared in the BT474c xenograft model. The observed efficacies of the three different schedules in terms of tumor growth inhibition were similar at the end of study (Fig. 5c). Intermittent dosing schedules that the model predicted to be equally efficacious were also confirmed to inhibit tumor growth to the same extent in an independent breast cancer xenograft model, MDA-MB-453 (Fig. 5d). Thus, the mathematical model predictions were validated. The blood glucose levels measured in animals after dosing these regimens are reported in Fig. 5e. It can be seen that higher intermittent dosing results in greater elevations of blood glucose concentration. However, the intermittent and continuous schedules were both well tolerated, with no overt toxicity or significant differences in body weight changes.

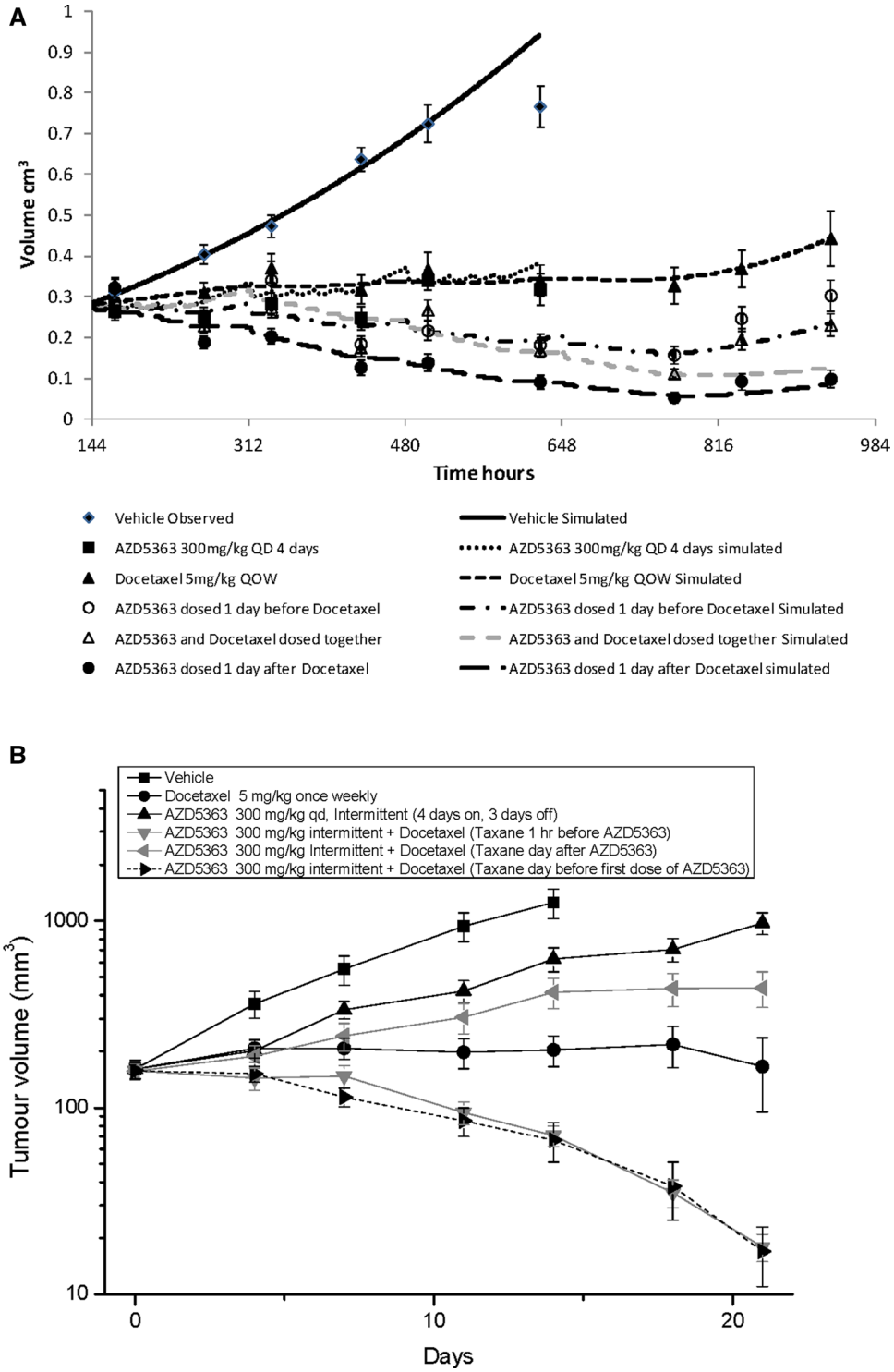

Fig. 4 Sequence dependence of efficacy when AZD5363 is combined with docetaxel. **a** Actual data and model fits for AZD5363 combination with docetaxel in BT474c xenografts. **b** Confirmation of sequence dependence in HCC-1187 xenografts

Conclusions

The AKT pathway is implicated in a number of cellular processes including both cell proliferation and survival. Therefore, inhibiting this pathway does not result in a single mode of action. The relationships between magnitude and duration of the pathway inhibition and the resulting phenotype could therefore be challenging to elucidate.

We demonstrate that adding mechanistic features to a descriptive model of drug-induced tumor growth inhibition makes it more representative of the disease biology and drug action. The concept of AKT inhibition effects

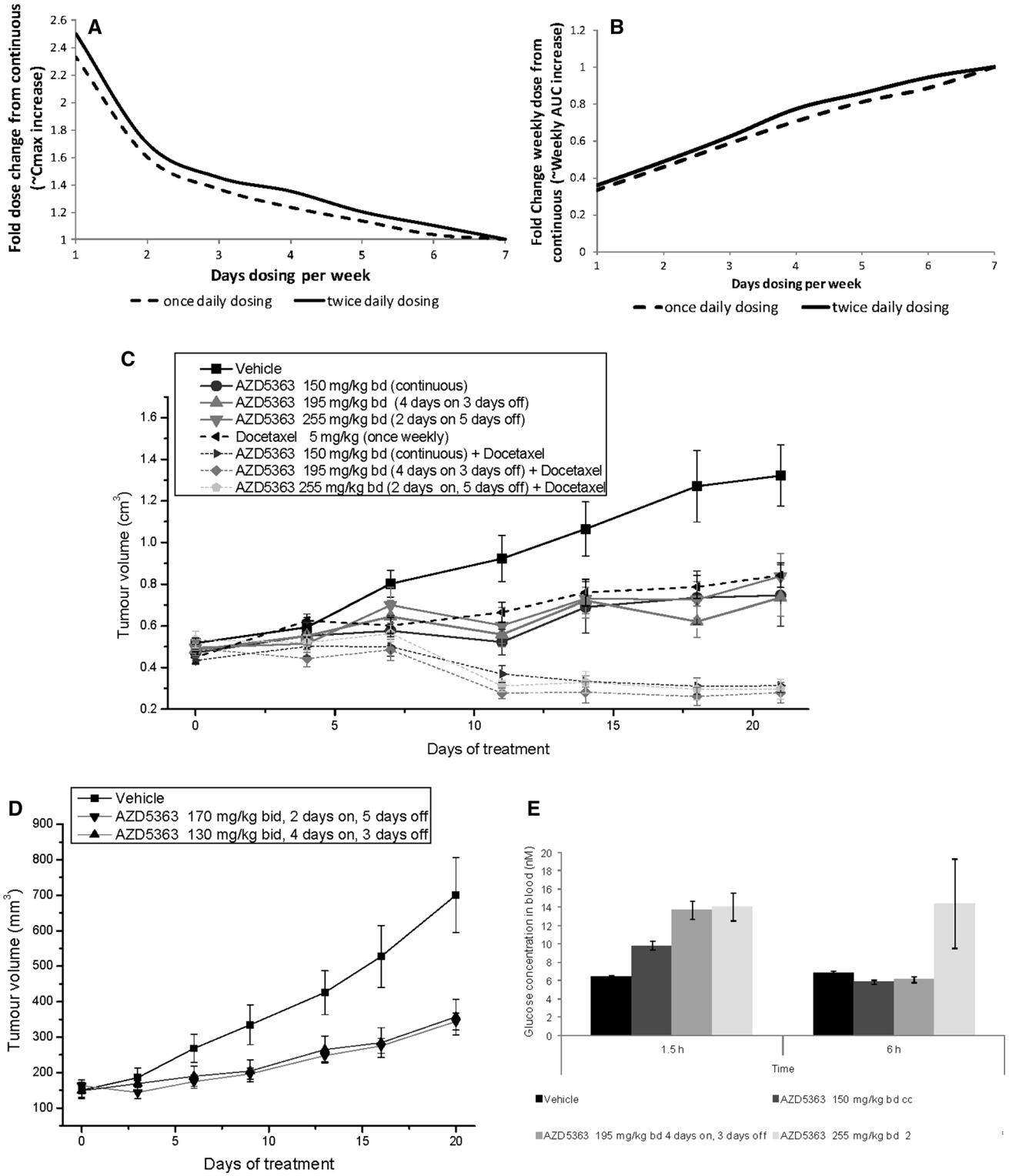

Fig. 5 Validation of model predictions of dose and schedule relationship. **a**, **b**, The model was simulated to estimate fold dose increase required for intermittent dosing to result in the same extent of tumor growth inhibition as continuous dosing. The plots show the relationship between the number of days dosing per week and the required dose increase. **c** Anti-tumor study in BT474c xenografts comparing continuous dosing to predict equi-efficacious intermittent dosing schedules. **d** Anti-tumor study in MDA-MB-453 xenografts comparing predicted equi-efficacious intermittent dosing schedules. In both xenograft models, the predicted equivalent efficacy was observed. **e** Blood glucose concentrations at 1.5 and 6 h after final dose, demonstrating dose-dependent elevations

on the inhibition of proliferation and induction of apoptosis has been validated against biomarker and efficacy data resulting from a range of doses and schedules of AZD5363. Modeling has enabled us to elucidate the relative balance of the anti-proliferative and pro-apoptotic consequences of AKT inhibition in a xenografted breast cancer cell line.

Mathematical modeling has also allowed us to capture, within a quantitative framework, the concept of combination of an AKT inhibitor with a taxane. This concept of sequence dependence, with AKT inhibition potentially antagonizing docetaxel through reduction in the proliferating compartment, has been validated as well. This again provides a clear rationale of how this AKT inhibitor should be combined with a taxane in the clinic. The validation of these scheduling approaches in several xenograft models demonstrates that this is not a cell line-dependent effect and therefore does have the potential for clinical translation.

Although the model is relatively complex, robust parameter estimates have been achieved. It should be noted that the parameter estimates from the three efficacy studies modeled (Tables 4, 5 and 6) vary very little between experiments pointing to a consistent PKPD–efficacy relationship. The two-compartment PK models are known parameter identifiable, as are the coupled indirect response models of the pharmacodynamics. The tumor growth model has been also shown to be parameter identifiable [18]. Hence, while mechanistic, the model is constructed in a pragmatic manner so that it is supported by the data. Furthermore, the model has incorporated a number of nonlinear relationships between dose, schedule and efficacy. The original Simeoni model, with its linear drug–effect relationship, would have predicted total drug per week to be predictive of efficacy, and this is clearly not the case here when we compare 100 mg/kg BD (1400 mg/kg/week) and 300 mg/kg QD for 4 days (1200 mg/kg/week). The model also contains the cell subpopulation idea of Ribba et al. [17], but here is linked directly linked to the total volume of the tumor and the assumption of the capacity limited delivery of blood to the tumor from the host. This allows the model to be built in the absence of histological data.

Through rational experimental design and mathematical modeling, we have been able to elucidate the schedule dependence of efficacy of an AKT inhibitor as a monotherapy and in combination with docetaxel. This has allowed us to identify and validate experimentally, different schedules with different drug exposures versus overall drug burden that deliver the same efficacy as judged by tumor growth inhibition. This has provided the rationale for different schedules to be investigated in the clinic that have the potential for the same anti-tumor efficacy but perhaps will have a different safety profile. The preclinical evidence presented here demonstrates the modest dose increases necessary (Fig. 5) to select a tolerated intermittent dosing schedule in preference to continuous dosing in the clinic. In the case of AZD5363, emerging clinical data suggest that intermittent dosing schedules reduce the frequency and severity of maculopapular skin rash with respect to the rates observed with continuous exposure to this compound and to the long half-life allosteric AKT inhibitor MK-2206 [4, 24]. However, our preclinical data suggest that another safety signal, hyperglycemia, may be more pronounced at higher doses (irrespective of whether continuous or intermittent) as this on-target effect appears to be related to Cmax. Preliminary clinical observations are consistent with increased rates of hyperglycemia at higher doses, but in all cases, this has been asymptomatic and adequately managed with oral metformin administration on dosing days. There have been no observed concurrent changes in HbA1c.

The results here also provide the rationale for dosing a taxane before AZD5363 on an intermittent schedule to achieve a good mechanistic combination effect. This can guide clinical development plans rather than compare such schedule options empirically in the clinic in large phase II trials. A focused experiment-model-predict-validate approach has achieved this in an efficient manner, with mathematical modeling being a tool for experimental design and hypothesis generation. Experimental validation has added credence to model predictions that will facilitate decision making for the clinical development program. There are implications for future drug discovery too in that the modeling approach described here can be applied, by substituting for relevant pathway biomarkers, to other targeted drugs as well as combinations. The evidence presented here and elsewhere suggests that equivalent or better efficacy may be achieved in the clinic, with better tolerability, by the use of intermittent dosing. Therefore, the automatic selection of candidate drugs with long half-lives limits this approach and should be reconsidered.

Acknowledgments AZD5363 was discovered by AstraZeneca subsequent to a collaboration with Astex Therapeutics (and its collaboration with the Institute of Cancer Research and Cancer Research Technology Limited).

Conflict of interest All authors are employees of AstraZeneca.

References

1. Vasudevan KM, Garraway LA (2011) AKT signaling in physiology and disease. Curr Top Microbiol 347:105–133
2. Hirai H, Sootome H, Nakatsuru Y, Miyama K, Taguchi S, Tsujioka et al (2010) MK-2206, an allosteric AKT inhibitor, enhances antitumor efficacy by standard chemotherapeutic agents or molecular targeted drugs in vitro and in vivo. Mol Cancer Ther 9:1956–1967
3. Davies BR, Greenwood H, Dudley P, Crafter C, Yu D, Zhang J et al (2012) Preclinical pharmacology of AZD5363, an orally bioavailable inhibitor of AKT: pharmacodynamics, antitumor

activity and correlation of monotherapy activity with genetic background. Mol Cancer Ther 11:873–887
4. Yap TA, Yan L, Patnaik A, Fearen I, Olmos D, Papadopoulos K et al (2011) First-in-man clinical trial of the oral pan-AKT inhibitor MK-2206 in patients with advanced solid tumors. J Clin Oncol 29:4688–4695
5. Lin J, Sampath D, Nannini MA, Lee BB, Degtyarev M, Oeh J et al (2013) Targeting activated AKT with GDC-0068, a novel selective AKT inhibitor that is efficacious in multiple tumor models. Clin Cancer Res 19:1760–1772
6. Davies AM, Ho C, Primo NL, Mack P, Gumerlock PH, Grandara DR (2006) Pharmacodynamic separation of epidermal growth factor receptor tyrosine kinase inhibitors and chemotherapy in non-small-cell lung cancer. Clin Lung Cancer 7:385
7. Martinelli G, Soverini S, Iacobucci I, Baccarini M (2009) Intermittent targeting as a tool to minimize toxicity of tyrosine kinase inhibitor therapy. Nat Clin Pract 6(2):68
8. Shah NP, Kantarjian HM, Kim DW, Réa D, Dorlhiac-Llacer PE, Milone JH et al (2008) Intermittent target inhibition with dasatinib 100 mg once daily preserves efficacy and improves tolerability in imatinib-resistant and -intolerant chronic-phase chronic myeloid leukemia. J Clin Oncol 26:3204–3212
9. Solit DB, She Y, Lobo J, Kris MG, Scher HI, Rosen N et al (2005) Pulsatile administration of the epidermal growth factor receptor inhibitor gefitinib is significantly more effective than continuous dosing for sensitizing tumors to paclitaxel. Clin Cancer Res 11:1983–1989
10. Wang S, Zhou Q, Gallo JM (2009) Demonstration of the equivalent pharmacokinetic/pharmacodynamic dosing strategy in a multiple-dose study of gefitinib. Mol Cancer Ther 8(6):1438
11. Wang X, Zhang L, Goldberg SN, Bhasin M, Brown V, Alsop DC et al (2011) High dose intermittent sorafenib shows improved efficacy over conventional continuous dose in renal cell carcinoma. J Transl Med 9:220
12. Kraus M, Wang Y, Aleksandrowicz D, Bachman E, Szewczak A, Walker D et al (2012) Efficacious intermittent dosing of a novel JAK2 inhibitor in mouse models of polycythemia vera. PLoS ONE 7:e37707
13. Fury MG, Solit DB, Su YB, Rosen N, Sirotnak FM, Smith RP et al (2007) A phase I trial of intermittent high-dose gefitinib and fixed-dose docetaxel in patients with advanced solid tumors. Cancer Chemother Pharmacol 59:467–475
14. Sangha R, Davies AM, Lara PN Jr, Mack PC, Beckett LA, Hesketh PJ et al (2011) Intercalated erlotinib-docetaxel dosing schedules designed to achieve pharmacodynamic separation: results of a phase I/II trial. J Thorac Oncol 6:2112–2119
15. La Rosée P, Martiat P, Leitner A, Klag T, Müller MC, Erben P et al (2013) Improved tolerability by a modified intermittent treatment schedule of dasatinib for patients with chronic myeloid leukemia resistant or intolerant to imatinib. Ann Hematol 92:1345–1350
16. Simeoni M, Magni P, Cammia C, De Nicolao G, Croci V, Pesenti E, Germani M, Poggesi I, Rochetti M (2004) Predictive pharmacokinetic-pharmacodynamic modelling of tumour growth kinetics in xenograft models after administration of anticancer agents. Cancer Res 64:1094–1101
17. Ribba B, Watkin E, Tod M, Girard P, Grenier E, You B, Giraudo E, Freyer G (2011) A model of vascular tumour growth in mice combining longitudinal tumour size data with histological biomarkers. Eur J Cancer 47:479–490
18. Evans N, Dimelow R, Yates J (2013) Modeling of tumour growth and cytotoxic effect of docetaxel in xenografts. Comput Methods Programs Biomed 114:e3–e13
19. Laplante M, Sabatini DM (2012) mTOR signaling in growth control and disease. Cell 149:274–293
20. Annovazzi L, Mellai M, Caldera V, Valente G, Tessitore L, Schiffer D (2009) mTOR, S6 and AKT expression in relation to proliferation and apoptosis/autophagy in glioma. Anticancer Res 29:3087–3094
21. Madhunapantula SV, Sharma A, Robertson GP (2007) PRAS40 deregulates apoptosis in melanoma. Cancer Res 67:3626–3636
22. Ribba B, Holford NH, Magni P, Trocóniz I, Gueorguieva I, Girard P, Sarr C, Elishmereni M, Kloft C, Friberg LE (2014) A review of mixed-effects models of tumor growth and effects of anticancer drug treatment used in population analysis. CPT Pharmacomet Syst Pharmacol 3:e113
23. Manning B (2004) Balancing AKT with S6K: implications for both metabolic diseases and tumorigenesis. J Cell Biol 167(3):399–403
24. Banerji U, Ranson M, Schellens J, Esaki T, Dean E, Zivi A, Van der Noll R, Stockman P, Marotti M, Garrett M, Davies BR, Elvin P, Hastie A, Lawrence P, Cheung SY, Stephens C, Tamura K (2013) Results of two Phase 1 multicenter trials of AZD5363, an inhibitor of AKT1, 2 and 3: biomarker and early clinical evaluation in Western and Japanese patients with advanced solid tumors. Abstract LB-66 AACR 2013